Applied Water Science (2020) 10:65
https://doi.org/10.1007/s13201-020-1152-0

ORIGINAL ARTICLE

A mechanistic insight into defluoridation of simulated wastewater applying bio-inspired sodium alginate bead

Prashil N. Thakre[1] · Shraboni Mukherjee[1] · Sucharita Samanta[1] · Sanghamitra Barman[2] · Gopinath Halder[1]

Received: 16 August 2018 / Accepted: 21 January 2020 / Published online: 28 January 2020

Abstract

The experiment successfully investigated fluoride (F^-) uptake capacity of bio-inspired sodium alginate bead (BISAB) using ZSM-5 as an adsorbent through a series of batch studies. The study conducted to observe impact of individual parameter on F^- adsorption reveals pH and adsorbent dose to have dominant effect in BISAB uptake as compared to time and temperature. Adsorbent prepared from ZSM-5 with high surface area and micropore volume can adsorb 92% of fluoride at optimized condition. Langmuir, Freundlich, D–R and Tempkin isotherms have been studied for fluoride adsorption. Among all models, Langmuir isotherm fitted exceptionally well over other models; this can be concluded from the regression coefficient obtained for Langmuir model which was very close to 1. The kinetic study suggests F^- adsorption onto prepared BISAB to follow pseudo-second-order kinetics of average rate constant 6.5475×10^{-4} g/fluoride per min. Thermodynamic parameters $\Delta H°$, $\Delta S°$ and $\Delta G°$ were found to be 10.167 kJ/mol, 29.35 J/mol and -4.71 to -13.4444 kJ/mol, respectively. The fluoride adsorption onto BISAB was endothermic reaction.

Keywords Adsorption · Defluoridation · Modeling · ZSM-5 · BISAB

Introduction

Fluoride is among the most plentiful elements found in groundwater globally which creates a notable difficulty in supplying safe consumable water. Intake of F^- within acceptable limit is crucial for maintaining healthy teeth and bones (Jagtap et al. 2011), while undue consumption of F^- often causes metabolic disruption in human being and animals like chronic skeletal and dental fluorosis, liver damage, thyroid disorder (Maity et al. 2018), neurological disorders, rickets, ossification of ligaments and tendons (Dong and Wang 2016). Therefore, World Health Organization (WHO) and Environmental Pollution Agency (EPA), India, have given a permitted limit of 1.5 mg/L of F^- concentration in consumable water (Chai et al. 2013). F^- occurrence in India was first reported in 1937 in Andhra Pradesh and then in 17 states of India mainly Rajasthan, Uttar Pradesh, Telangana, Madhya Pradesh, Gujarat and West Bengal (Mukherjee et al. 2018a).

Several commercial methods are already being designed for F^- removal in aqueous solution like adsorption (Daifullah et al. 2007; Mukherjee et al. 2017), ion exchange (Meenakshi and Viswanathan 2007), precipitation (Akbar et al. 2008), electrodialysis (Lahnid et al. 2008), Donnan dialysis (Tor 2007), reverse osmosis (Sehn 2008) and nano-filtration (Liu et al. 2007), etc. Nonetheless, membrane-based techniques and ion exchange involve higher maintenance as well as operational expenses, complicated procedure and production of toxic sludge during defluoridation from aqueous solution. The out-dated techniques of precipitation and coagulation have been applied toward F^- removal from water, wherein Nalgonda process has been one of the most broadly used processes to treat fluorinated water across the world. However, production of higher degree of lasting aluminum concentration often between 2 and 7 mg/L is considered as a major drawback of these processes (Ghorai and Pant 2005; Mohapatra et al. 2004). Owing to the aforementioned shortcomings, adsorption-based F^- removal is promising as well as viable due to the availability of various adsorbents at low pollutant concentration, not-so-complicated operation, easy maintenance and effectual performance. Various adsorbents

✉ Gopinath Halder
gopinathhaldar@gmail.com

[1] Chemical Engineering Department, National Institute of Technology Durgapur, M. G. Avenue, Durgapur, West Bengal 713209, India

[2] Chemical Engineering Department, Thapar University, Patiala, Punjab 147004, India

till date have been reported for F^- removal from water, viz. alumina (Ghorai and Pant 2005), minerals and metal oxides (Mohapatra et al. 2004; Tor 2006), carbon (Ramos et al. 1999), zeolites (Onyango et al. 2004), clays (Fan et al. 2003), industrial and agricultural wastes (Chidambaram et al. 2003; Mukherjee and Halder 2018), etc. Although activated carbon is a popular adsorbent for F^- removal, commercial activated carbon has a high operating cost which, at high water flow rate, greatly increases if there is no carbon regeneration unit (Figueiredo et al. 2005).

Therefore, of late more attention is paid toward development of an effective adsorbent such as clays, tree barks, petroleum coke, alum sludge, wood charcoal, red mud, nanoparticles and bio-char-based alginate beads (Kirk 1980; Çengeloğlu et al. 2001; Srimurali et al. 1998; Pradhan et al. 1999; Asyhar et al. 2002; Yakun et al. 2011). Owing to their low price, the ease of obtainability and effectual F^- removal from water, these alternative waste materials are being utilized and reported. Various functional groups existing on the surface of a biomass-based adsorbent, namely carboxyl, hydroxyl, amide, amines and carbonyl, might be involved in the physicochemical interaction of F^- (Mukherjee et al. 2018a). Several experiments have reported the removal of other metals (Yu et al. 2017), dye (Rocher et al. 2010) and organic pollutants (Hammouda et al. 2015) from aqueous solution with the help of nanoparticle-impregnated alginate beads as well as carbon-based alginate beads. Therefore, in the current study, we concentrated on the following objectives:

- To explore F^- adsorption capability of BISAB (bio-inspired sodium alginate beads) under different chemical as well as physical conditions. For this purpose, a batch experimental study was carried out for analyzing impact of process parameters, viz. adsorbent dose, contact time, pH, temperature, initial F^- concentration.
- To determine the best-fit isotherm and kinetic model and thermodynamic study of the experimental data using bio-inspired sodium alginate beads.

Materials and methods

Chemicals and glasswares

Rice husk-based nanoparticle was prepared in laboratory scale following standard procedure mentioned by Ghasemi and Younesi (2011) and also reported by different researchers later on (Mukherjee et al. 2018b). Sodium alginate [$(C_6H_7NaO_6)_x$, 91%] food grade was obtained from Lobal Chemie, India. Sodium fluoride (NaF, 99%), hydrochloric acid (HCl, 37%) and sodium hydroxide pellets (NaOH, 98%) were obtained from Merck, India. Calcium chloride pellets ($CaCl_2$, 98%) were purchased from Fisher Scientific. Deionized water (Millipore) was utilized for the experimental purpose.

Development of adsorbent NZSM 5

Synthesis of classified porous NZSM-5 was conducted on the basis of layer via one-pot method. Firstly, a gel was prepared by mixing 1.10 g sodium aluminate with 5.25 g fumed silica and 1.5 g NaOH in 100 mL distilled water (Coruh and Ergun 2009). These were uniformly stirred for 60 min by the addition of 5 mL 20% tetrapropylammonium hydroxide dropwise in a parent gel solution. Later for betterment of the prepared gel, it was kept in an autoclave reactor for 4 days at 160 °C for crystallization. Then, it was collected within 0–96 h to analyze the influence of nucleation rate and crystallinity. Lastly, the blend product was filtered and washed with the distilled water to make its pH value to 8.0. The filtrate was then kept in a hot air oven at 80 °C for 24 h (Arief et al. 2008).

For modification, 2 g NZSM-5 was added in the known concentration of 200 mL HDTMA-Br aqueous solution and agitated in incubator at 200 rpm for 24 h and 30 °C. For determining the effect of 0.5–2.5 g/L concentration, HDTMA-Br was used. This was followed by centrifuging the functionalized NZSM-5 (F NZSM-5) for 35 min at 15,000 rpm and then rinsed in deionized water till Br^- was detected. The $AgNO_3$ was added in washed water sample for the detection of Br^- as the yellowish formation of precipitation formed. Then, FNZSM-5 particles were oven-dried for 12 h at 60 °C which were later used for the removal of F^-.

Preparation of bio-inspired sodium alginate beads (BISABs)

Sodium alginate powder was mixed with deionized water (w/v, 1%) followed by the addition of rice husk-derived nanoparticles to the solution of sodium alginate in the ratio of 1:1. The mixture was stirred well to get a uniform mixture of sodium alginate and nanoparticles using mechanical stirrer. The mixture was then mixed with 1% $CaCl_2$ solution in the form of drops using a 5-mL syringe for forming uniformly sized beads. These were then separated from the solution for hardening after 24 h, followed by washing with deionized water (Wang et al. 2015) and dried. After drying, the typical size of bio-inspired sodium alginate beads was found to be about 2.7–2.9 mm in diameter.

Batch adsorption experiments

Batch sorption studies were conducted by using F^- concentration of 10 mg/L, and adsorbent doses were varied in between 0.02 and 0.1 g/L. pH was maintained between 2.0

and 10.0 using 1.0 mol/L HCl or 1.0 mol/L NaOH which was monitored with a Delta 320 pH meter (Mettler-Toledo). At constant temperature, batch adsorptive experiments were carried for 24 h. After adsorption equilibrium, the solution was filtered, using filter paper to determine the F^- ion concentration.Through F^- ion selective electrode, the adsorption capability of BISAB was determined by Eq. (1):

$$q_e = \frac{C_0 - C}{W} \times V \quad (1)$$

where q_e indicates adsorption capacity of BISAB (mg/g); C_0 and C are initial and final F^- concentrations in solution (mg/L). W refers to weight of dry sodium alginate beads (g), whereas V refers to BISAB's volume in synthetic solution (L).

Instrumental characterization of nano-zeolite ZSM 5

Scanning electron microscope (SEM) (JEOL, JXA-840A) aided in analyzing the surface morphology and structure of BISAB. In addition, to determine the elements present on BISAB surface before and after F^- uptake, the energy-dispersive X-ray (EDX) was taken at 10 keV voltage (Vázquez et al. 2012).

Brunauer–Emmett–Teller (BET) analysis was used for further characterization of a microstructure of BISAB. The average pore diameter and BET surface area were determined by means of gas adsorption pore size analyzer (NOVA 1000e, Quantachrome Ins.).

Results and discussion

SEM–EDX and BET analyses

BISAB's surface texture before and after F^- uptake is shown in Fig. 1a–d wherein the surface of BISAB was spherical, porous and smooth, which increases the F^- adsorption capacity along with specific surface area of BISAB (Travlou et al. 2013). EDX analysis of BISAB after F^- adsorption is shown in Fig. 1b; there was a noticeable F^- content after adsorption as seen in the EDX spectrum, which suggested BISARB to be an effective adsorbent for F^- uptake (Paudyal

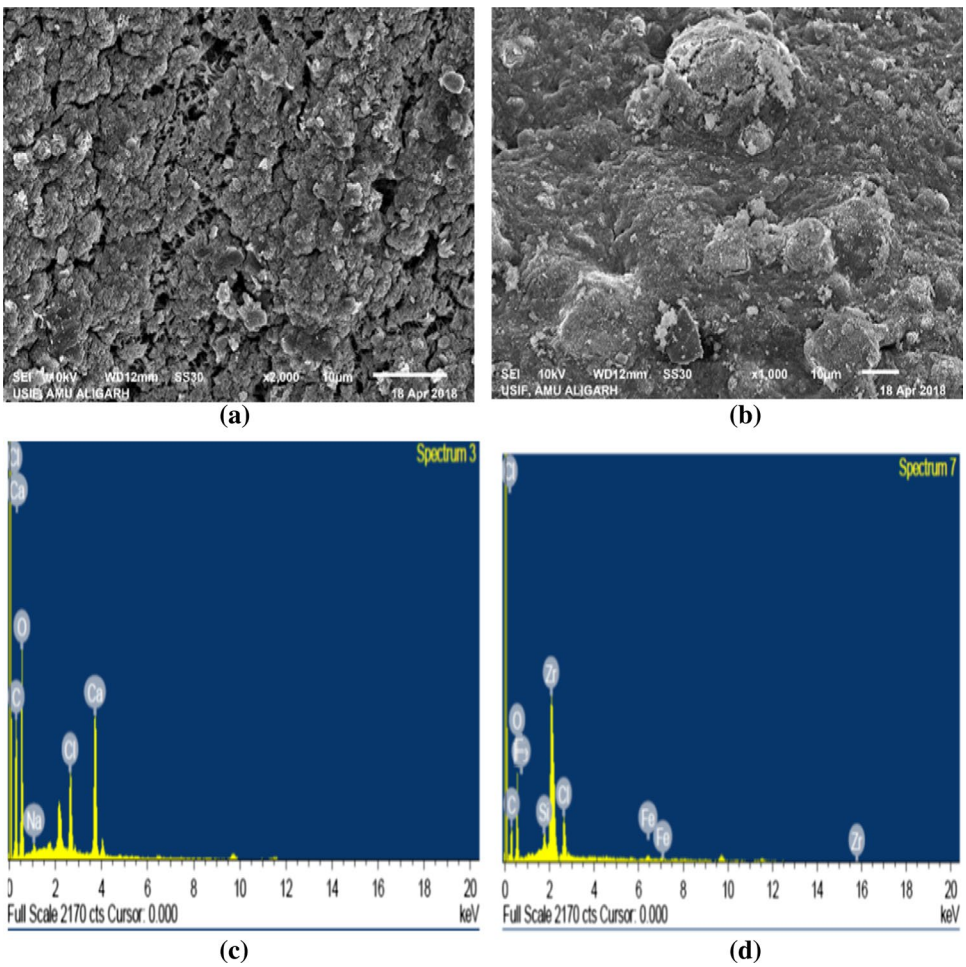

Fig. 1 **a–d** SEM and EDX spectra of BISAB before and after fluoride adsorption

Table 1 Surface characterization of BISAB

Adsorbent	BET surface area (mg/g)	Average pore diameter (nm)
BISAB	17.64	9.17

Table 2 a, b Elemental analysis of fluoride over BISAB through EDX

Elements	Weight (%)
(a)	
C	33.22
O	52.86
Na	0.62
Cl	4.00
Ca	9.30
Total	100.00
(b)	
C	29.64
O	36.38
Si	0.93
F	4.38
Fe	5.93
Zr	22.74
Total	100.00

et al. 2012). Table 1 presents the surface area and average pore diameter of BISAB. BISARB had higher surface area than BISAB with an analogous mean pore diameter, and hence, BISARB resulted in adsorbing higher percentage of F^-. The elemental analysis of BISAB before and after F^- uptake is shown in Table 2a, b.

FTIR analysis of BISAB and BISARB

FTIR analysis of BISAB before and after F^- uptake is depicted in Fig. 2b. For the adsorbent bending and stretching vibration of the adsorbed water, broad bands were assigned at 1062 cm^{-1}, 1636 cm^{-1} and 3443 cm^{-1} and bending vibration of metal (M–OH), respectively (Tomar et al. 2013). The peak obtained at 1419 cm^{-1} represented carboxyl group (–C=0). The peak at 1319 cm^{-1} indicated bending and stretching of absorbed water C–H (Karthikeyan et al. 2011). Figure 2 clearly shows a shift in bands at 450 cm^{-1}, 1062 cm^{-1}, 1636 cm^{-1}, 3442 cm^{-1} to 430 cm^{-1}, 1060 cm^{-1}, 1637 cm^{-1} and 3456 cm^{-1} after F^- uptake. For hydroxyl group on the adsorbent, the broad band was indicative of stretching vibration at 3443 cm^{-1}, that is, adsorbed water and metal oxides. After adsorption, intensity of hydroxyl (–OH) band decreases at 3443–3456 cm^{-1}, but peak's shape changed which resulted in higher frequencies of F^--loaded adsorbent causing F^- uptake/exchange. For defluoridation of water, the hydroxyl group was possibly responsible. BISARB after F^- uptake was assigned to M–F with band at 542 cm^{-1}, and M–O was assigned at band of 450 cm^{-1}.

Influence of parameters on fluoride uptake by ZSM 5

Influence of pH

F^- adsorption on BISAB was analyzed at pH value of 2–10. Maximum sorption of F^- on BISAB was calculated as 90.9% at pH 4, i.e., in acidic medium, while adsorption capacity went on decreasing as the as pH value went on increasing, i.e., in alkaline medium as shown in Fig. 3a. The lowest adsorption percentage was about 65% found to be at pH 10. The F^- ions adhered onto BISAB surface, wherein an ion exchange took place between transportable OH^- ion present nearer to the surface of BISAB (Fan et al. 2003). There was maximum F^- removal in acidic medium since the surface of BISAB got highly protonated and became positive in acidic medium, which was attributed to attraction of negatively charge ions (Gao et al. 2009), whereas increasing pH decreased the adsorption capacity due to more OH^- ions which competed with negatively charged F^- ions. The repulsive force caused a decrease in sorption capacity of OH^- and F^- ions in alkaline medium. Thus, synthesized BISAB is effective for F^- removal from simulated wastewater at neutral to lower pH value.

Influence of contact time

The effectiveness of adsorbent was calculated by studying the adsorption kinetics. The relationship between adsorption capacity (mg/g) and respect to time (min) at different initial concentrations of fluoride is shown in Fig. 3b. During the sorption process, a two-step mechanism was followed as illustrated in Fig. 3b. The first mechanism result shows that there is rapid adsorption of fluoride ion on BISAB within first 90 min, after which stability was gradually achieved. The F^- removal after 90 min was 84.3%, 80.6%, 88%, 55.8% and 80.6% at initial concentrations of 4, 8, 12, 16 and 20 mg/L, respectively. These experimental data were further used in kinetic modeling of F^- adsorption in aqueous solution to determine pseudo-first-order and second-order models for estimating R^2 value and to find appropriate dynamic model. The rate constant (K) of F^- sorption constant was determined for different reaction temperatures and initial F^- concentration from batch experimental study.

Influence of initial concentration

Impact of initial F^- concentration over BISAB was studied at varying concentrations, viz. 5, 10, 15 and 20 mg/L using 0.1 g BISAB dose at 30 °C. The study revealed that with increasing initial concentration, removal percentage

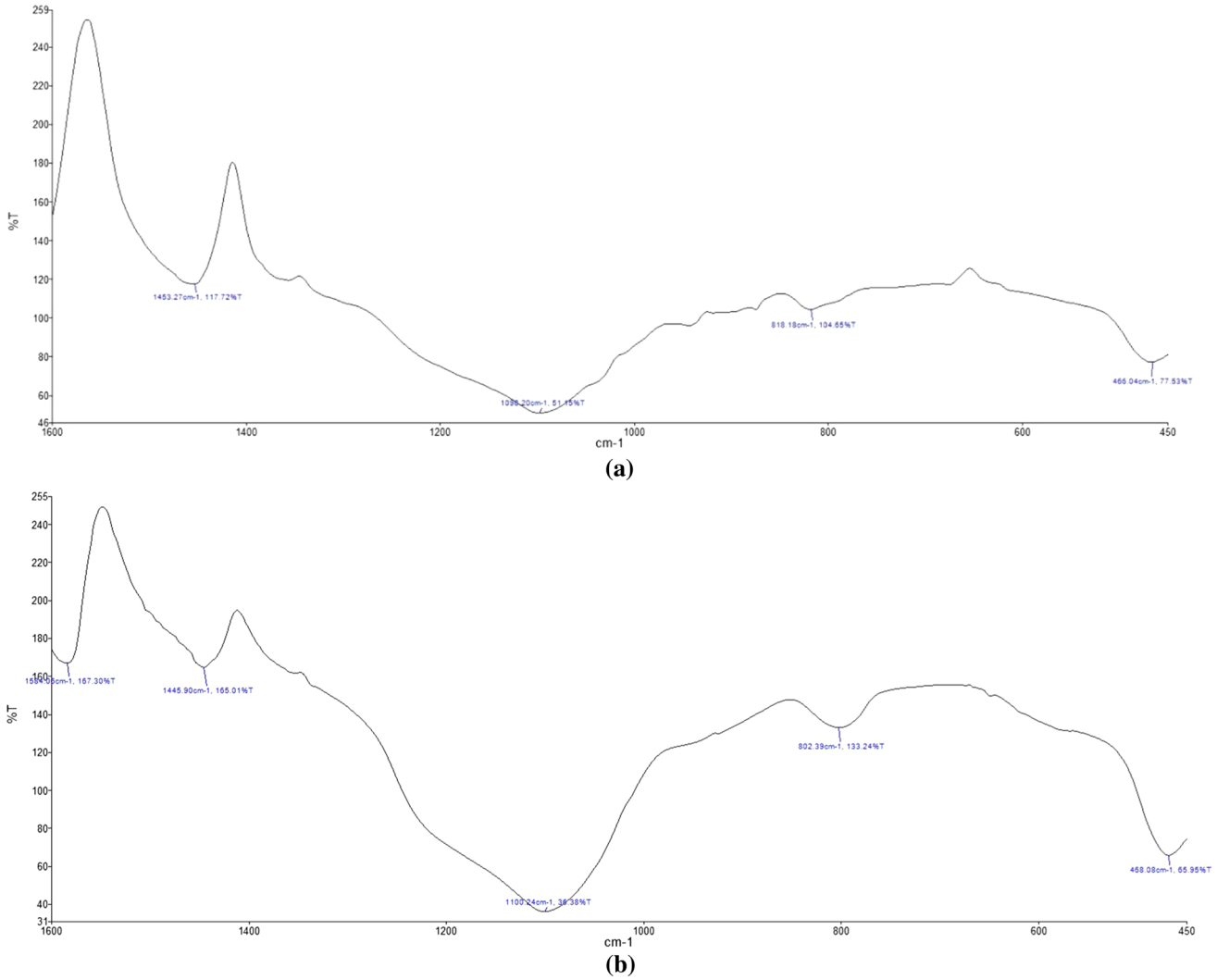

Fig. 2 FTIR spectra for BISAB (**a**) before and (**b**) after fluoride adsorption

of F^- also increases as shown in Fig. 3c. This result is consistent and matches with previous reports on adsorption of fluoride ions in synthetic solution (Liu et al. 2013).

Influence of adsorbent dose

F^- adsorption onto BISAB was determined by varying the dose of adsorbent (0.4, 0.6, 0.8, 1.0, 1.2, 1.4 and 1.5 g/50 mL) while keeping initial fluoride concentration (100 mg/L), pH (9.0) and temperature (34 °C) constant at a contact time of 110 min as shown in Fig. 3d. The rate of sorption increased from 70 to 95%, with BISAB dose increasing from 0.4 to 1.5 g per 50 mL at equilibrium time. This is owing to more accessibility of surface area and sorption sites, while the unit adsorbed F^- decreased with increasing BISAB dose as shown in Fig. 3d.

Influence of temperature

Along with other factors, temperature too plays a vital role in an adsorption process. In this case, temperature was varied from 49.85 to 85 °C. Figure 3e depicts the influence of temperature on F^- removal by BISAB. Higher temperature causes enhanced binding of F^- ions onto BISAB surface (Arief et al. 2008). As seen in the graph, optimal temperature was observed as 60 °C with maximum 90% removal, after which it gradually lowered with rise in temperature up to 70 °C. This is indicative of the fact that the van der Waal's forces are quite weaker at low temperature causing lowered interaction between BISAB and F^- ions. Hence, medium temperature promoted enhanced adherence of the F^- ions onto BISAB surface because of comparatively stronger van der Waal's forces. Very high temperatures often cause breakage in

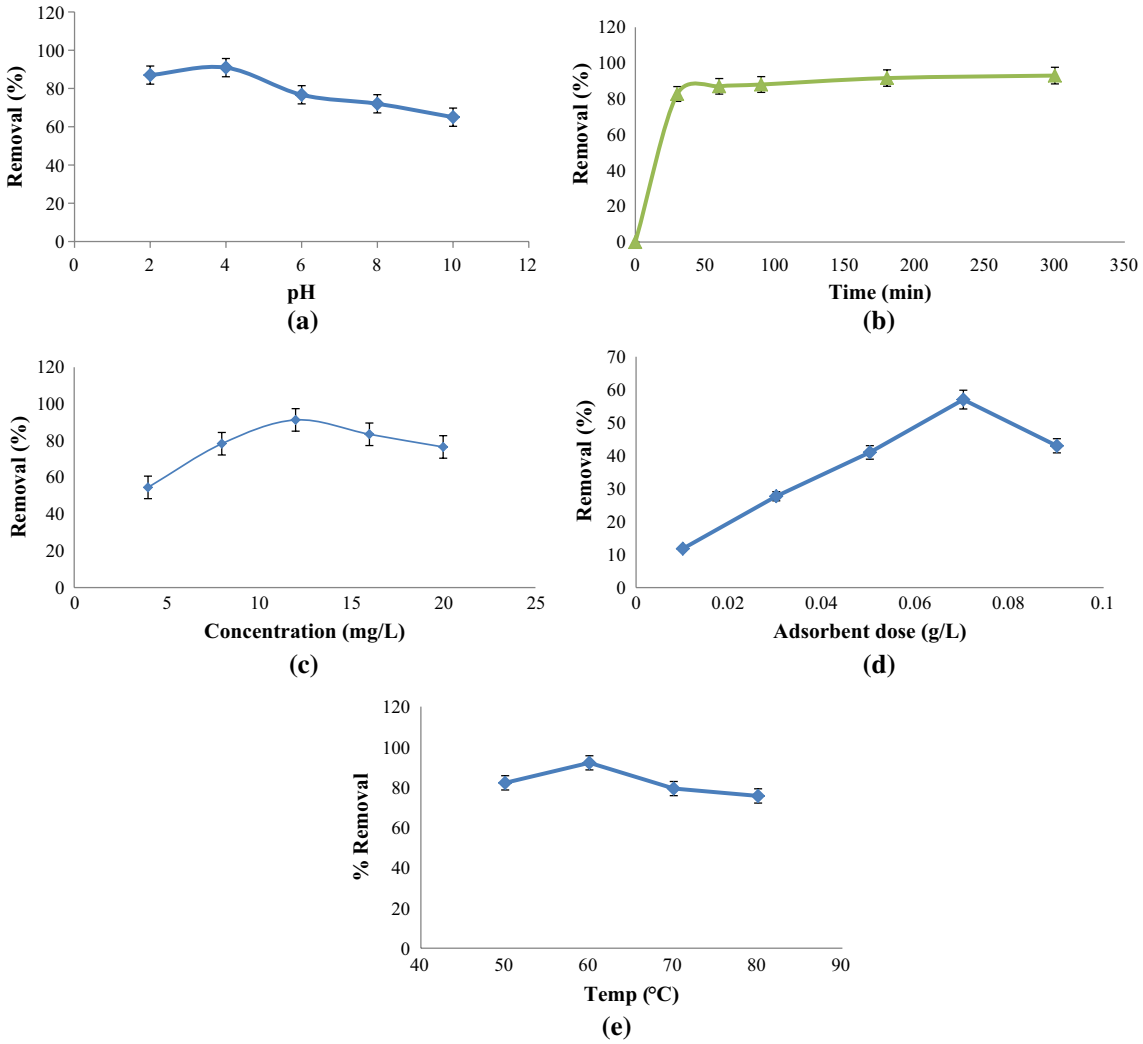

Fig. 3 **a–e** Effect of individual parameters

the ionic bonds which reduce sorption efficacy of sorbent (Mukherjee and Halder 2016).

Adsorption isotherm

In adsorption studies, the relationship between quantity of adsorbate sorbed on adsorbent surface and its solution concentration at fixed temperature is described by adsorption isotherm. Various sorption models have been investigated in several studies; however, the current experimental work focused on mainly Langmuir, D–R, Freundlich and Temkin models, wherein q_e (i.e., adsorption capacity per unit mass of BISAB) is a common parameter used by the first 3 isotherm models.

Langmuir isotherm

This model presumes homogeneous adsorption to occur over an adsorbent's monolayer surface devoid of any interaction among the adsorbed species. Linearized equation of this isotherm is expressed in Eqs. (2) and (3) (Langmuir 1915):

$$q_e = \frac{Q_{max} K_L C_e}{1 + K_L C_e} \tag{2}$$

$$\frac{1}{q_e} = \frac{1}{Q_{max} K_L C_e} + \frac{1}{Q_{max}} \tag{3}$$

where q_e (mg/g) is adsorption capacity at equilibrium; C_e is F^- concentration at equilibrium solution (mg/L); Q_{max}

(mg/g) refers to adsorption capability at saturation; and K_L is Langmuir constant for adsorption which is related to free and binding energy of adsorption.

Freundlich isotherm

This model is based on the fact of exponential decaying of adsorption site energy distribution and is applicable for non-ideal adsorption on heterogeneous surfaces depicting multilayer adsorption. The mathematical expression for Freundlich isotherm is written as Eq. (4) (Santra et al. 2014):

$$\lg q_e = \frac{1}{n} \lg C_e + \lg K_F \tag{4}$$

where K_F refers to Freundlich adsorption constant [(mg/g) $(L/mg)^{1/n}$], n indicates heterogeneity factor and Freundlich constant related to adsorption capacity. n and K_2 value are estimated from slope and intercept by plotting linear plot between C_e and log q_e, respectively.

The correlation constant (R^2) and isotherm constant for linear Freundlich and Langmuir isotherms are given in Table 2. The results suggest superior fit of Langmuir isotherm over Freundlich from the linearly plotted graphs shows high $R^2 = 0.9986$ value for the Langmuir isotherm for F^- adsorption by BISARB from synthetic solution.

Temkin isotherm

This model was used for analyzing the F^- sorptive potential of BISAB. The derivation of this isotherm presumes fall in heat of adsorption to be linear rather than logarithmic. Tempkin isotherm has been usually used as shown in Eq. (5) (Cheng et al. 2014; Zhang et al. 2014):

$$q_e = \left(\frac{RT}{b_T}\right) \ln(K_T C_e). \tag{5}$$

Equation (6) is the simplified version of Eq. (5):

$$q_e = \beta \ln \alpha + \beta \ln C_e \tag{6}$$

where $\beta = (RT)/b$, T (K) refers to absolute temperature and R 8.314 J $(mol\ K)^{-1}$ indicates universal gas constant. The constant b defines heat of adsorption (Yu et al. 2013; Wu et al. 2001). Linearized equation of Tempkin isotherm was used for estimating experimental data, and it provided a good fit to the fluoride adsorption data for BISAB. The results are given in Table 3. The correlation coefficients R^2 obtained from Tempkin model were comparable to that obtained of Langmuir and Freundlich equations, which elucidate application of Tempkin model to F^- sorption onto BISAB as shown in Fig. 4c.

Dubinin–Radushkevich (D–R) isotherm

This isotherm is calculated for the analysis of apparent adsorption energy and the porosity of an adsorbent. The linear equation of D–R isotherm is presented in Eq. (7):

$$\ln q_e = \ln q_D - 2B_D \left[RT \ln\left(1 + \frac{1}{C_e}\right)\right]^2 \tag{7}$$

where q_D (mg/g) is the D–R isotherm constant related to amount of F^- sorbed onto BISAB.

Adsorption kinetics

In the case of fluoride adsorption over BISAB, the time-dependent analysis for two diverse sorption kinetic models,

Table 3 a–d Parametric study of Langmuir, Freundlich, Temkin and D–R isotherms of BISAB at 333 K

Ion	Isotherm	Q_m (mg/g)	b (mg^{-1})	R^2
(a)				
F^-	Langmuir	34.2465	0.0298	0.9986
Ion	Isotherm	K_f (mg/g)	$1/n$	R^2
(b)				
F^-	Freundlich	1.1174	1.1698	0.9823
Ion	Isotherm	K_T	B_T	R^2
(c)				
F^-	Temkin	336.32	0.4894	0.8201
Ion	Isotherm	K_{ad}	q_s	R^2
(d)				
F^-	Dubinin–Radushkevich	−0.0027	8.9728	0.9996

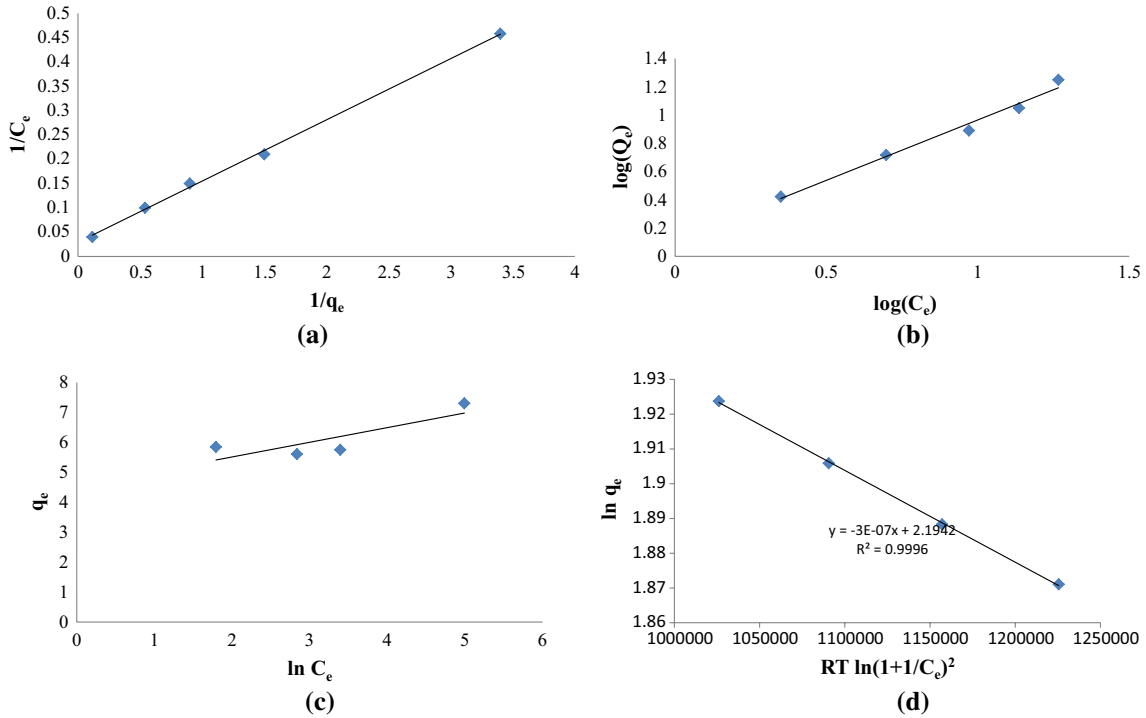

Fig. 4 **a** Langmuir, **b** Freundlich, **c** Temkin, **d** D–R isotherm studies

viz. pseudo-first order and second order, was studied at 30 °C (Zhang et al. 2014).

The linear expression of pseudo-first order is given in Eq. (8) (Cheng et al. 2014):

$$\log(q_e - q_t) = \log q_e - \frac{K_1 t}{2.303} \quad (8)$$

where K_1 and q_t refer to pseudo-first-order equation's rate constant at equilibrium (min^{-1}) and sorption capacity at a time (t) (mg/g).

The calculated value q_e, K_1 and correlation coefficient for the pseudo-first-order kinetic model at 30 °C are given in Table 4.

The linearized equation of pseudo-second order is given as Eq. (9) (Yu et al. 2013):

Table 4 Kinetic parameters: (a) pseudo-first-order and (b) pseudo-second-order kinetic parameters

Kinetic model	Initial fluoride concentration (mg/L)	Rate constant (min^{-1})	R^2
(a)			
Pseudo-first order	4	−0.030169	0.8777
	8	−0.4767	0.9651
	12	−0.0299	0.9892
	16	−0.0310	0.9067
	20	−0.0283	0.9092
Kinetic model	Initial fluoride concentration (mg/L)	Rate constant (g/mg min)	R^2
(b)			
Pseudo-second order	4	0.07651	0.995
	8	0.03013	0.9968
	12	0.01983	0.9999
	16	0.023015	0.9992
	20	0.0252	0.9983

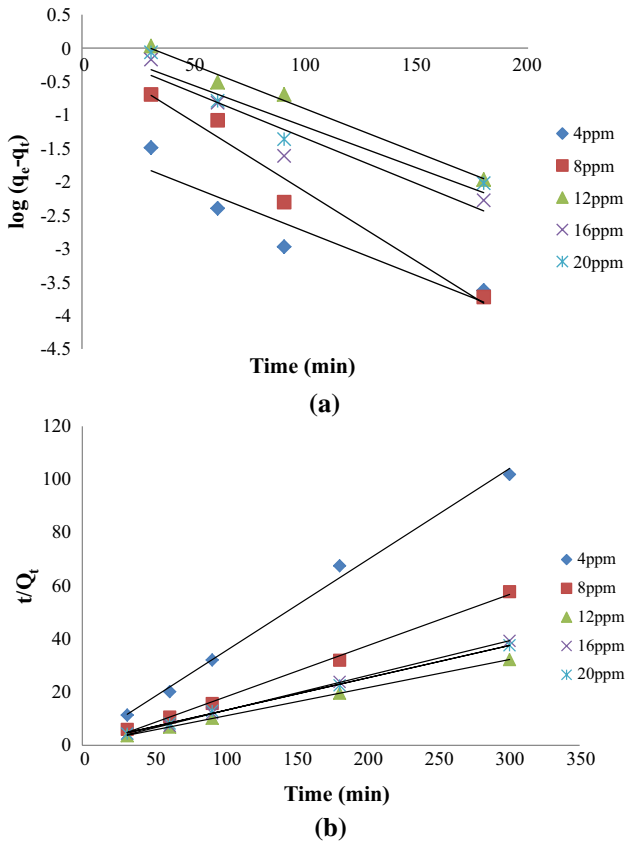

Fig. 5 **a** Pseudo-first-order and **b** Pseudo-second-order kinetic studies

$$\frac{t}{q_t} = \frac{1}{K_2 q_e^2} + \frac{t}{q_e}. \tag{9}$$

Plots of t/q_t versus t for F^- adsorption are depicted in Fig. 5a. The rate constants for both the kinetic models are presented in Table 4. Value of R^2 for pseudo-second-order kinetic model was much greater than pseudo-first-order kinetic model. Thus, experimental result suggested that pseudo-second-order kinetic model suggested better explanation on F^- adsorption than pseudo-first-order kinetic model. Second-order kinetic model assumes rate-limiting step by chemical adsorption in the adsorption process (Wu et al. 2001).

Adsorption thermodynamics

In a low concentration, the activity coefficient remains constant according to Henrys law. The thermodynamic parameters are calculated by using Eqs. (10) and (11):

$$\Delta G^\circ = -RT \ln K_C \tag{10}$$

$$\ln K_C = \frac{\Delta S^\circ}{R} - \frac{\Delta H^\circ}{RT} \tag{11}$$

Table 5 Thermodynamic parameters of BISAB at 313 K

Initial fluoride concentration (mg/L)	Temperature (K)	ΔG° (KJ/mol)	ΔH° (KJ/mol)	ΔS° (KJ/mol)	R^2
10	313	1.4322	41.68	0.4856	0.9313

where R, T and K_C refer to gas constant, temperature and equilibrium constant, respectively. The thermodynamics parameters suggested F^- adsorption to be spontaneous process as $\Delta G^\circ < 0$, and $\Delta H^\circ = 41.68$ kJ/mol; the fluoride adsorption process is an endothermic process according to solid–liquid adsorption theory. Solute molecules tend to lose a degree of freedom from liquid phase to solid–liquid interface leading to decrease in entropy, in line with theory $\Delta S^\circ < 0$ (Table 5).

Effect of competing ions

In general, a contaminant removal phenomenon tooled by an adsorbent is governed by a specific mode of interface interaction. The active adsorbing sites present on the surface of an adsorbent are crowded by the adsorbate ions, which can be evident from initial higher rate of adsorption followed by an intermediate step where minimal increment can be seen which continues till the adsorbent particles are saturated.

In the present batch mode experimental process, the maximum removal was seen in the case of the acidic solvents due to their involvement in increasing the H^+ ions in the solutions which competed with the adsorbate ions in desorption. In the acids, desorption of F^{-1} was greater due to their weak bond which was easily replaced with advancement of H^+ in the solution. The adsorbent was regenerated with 0.01 M NaOH in order to remove excess of H^+ ions from its surface. On the other hand, basic solution was unable to remove efficiently since the adsorbent surface was pre-composed with OH^- which will eventually hydroxide ions present in the solution. Besides all this phenomenon, it is seen that F^{-1} is a highly electro-negative ion which has a high electron affinity toward the highly electro-positive Na^+ rather than Si^{4+} and other ions present in the bio-inspired alginate beads, probably for which the favorable removal efficacy of the fluoride ion by the nanoparticle-incorporated alginate beads was uninterrupted through-out the adsorption process.

Regeneration study

The regeneration of porous sodium alginate is essential to make a cost-effective and eco-friendly procedure. The regeneration study was carried out following proper

protocol reported by Qiusheng et al. (2015). The result of pH effect on fluoride adsorption by porous sodium alginate beads showed that the adsorption capacity of alginate beads decreased gradually with the increase in pH and was lower in alkaline solution (Fig. 3a). In order to improve desorption of the adsorbent, the desorption experiments were carried out in NaOH alkaline solution at high temperature range between 70 and 80 °C. Drained alginate beads were dipped in 0.01 M NaOH for 1 h and washed repeatedly with deionized water for neutralization and then transferred to a beaker containing the stirring effect for activation at high temperature range between 70 and 80 °C for 3 h. The desorption efficiency was about 52.58% after three cycles.

Safe disposal

Safe disposal of the used alginate beads as adsorbents must be recognized to avoid any kind of further environmental contamination. The fluoride ions need to be completely eliminated from the used alginate beads as adsorbents, even after decomposition of the adsorbents, to avoid the remaining chances of leaching of fluoride ions into the soil, thereby contributing to ecological threat. Different approaches have been reported for safe disposal of metal or non-metal loaded adsorbents. In this experimental analysis, the used alginate beads as adsorbents were securely disposed off as per the practice recommended by Mukherjee et al. (2017). At first, the alginate beads were dried at 60 °C in an air oven monitored by incineration of the dried biomasses at 200 °C. Approximately 5 g of the ash obtained from each incinerated biomass was mixed together and then added to 25 mL deionized water. This mixture was continuously stirred for 24 h (Iyenger 2005). Then, the filtrate was collected and examined to determine the residual fluoride concentration. It was observed after following this method that no leaching of fluoride ions happened. This incinerated ash can be used for road construction or brick manufacture with additional modifications if required.

Conclusions

The current study successfully investigated adsorption of fluoride over BISAB from simulated wastewater. The maximum percentage removal was about 92% at adsorbant dose of 5 mg with F^- concentration of 10 mg/L, and pH and temperature of the solution were 4 and 333 K, respectively, within 4 h contact time. F^- sorption was best explained by the Langmuir isotherm over Freundlich, Temkin and D–R isotherms. Higher correlation coefficient of pseudo-second-order reaction is greater than that of pseudo-first-order one, showing that fluoride sorption process obeys pseudo-second-order reaction. Spontaneity, randomness and feasibility of fluoride sorptive process were obtained from thermodynamic parameters. Irreversible and endothermic nature of F^- sorption is indicative of the negative value of Gibbs free energy. Abundance of functional groups such as primary and tertiary amides which are accountable for F^- sorption were suggested by FTIR spectra. From the optimum removal efficacy in the batch mode adsorption study, it is well observed that bio-inspired alginate beads proved to be a productive adsorbent for the efficient removal of contaminants. Using this efficient bio-inspired alginate bead, the column study can be done more efficiently in the future for scaling up in real practices in industries.

Acknowledgements Authors express their sincere gratitude to Chemical Engineering Department, NIT Durgapur and Thapar University for their support and cooperation toward successful completion of the work. The technical support of the laboratory staffs is also acknowledged.

References

Akbar E, Maurice SO, Aoyi O, Shigeo A (2008) Removal of fluoride ions from aqueous solution at low pH using schwertmannite. J Hazard Mater 152(2):571–579

Arief VO, Trilestari K, Sunarso J, Indraswati N, Ismadji S (2008) Recent progress on biosorption of heavy metals from liquids using low cost biosorbents: characterization, biosorption parameters and mechanism studies. CLEAN Soil Air Water 36:937–962

Asyhar R, Wichmann H, Bahadir M, Cammenga HK (2002) Equilibrium adsorption studies of activated coke towards phenol and 4-nitrophenol. Fresenius Environ Bull 11(6):270–277

Çengeloğlu Y, Kir E, Ersoz M (2001) Recovery and concentration of Al(III), Fe(III), Ti(IV) and Na(I) from red mud. J Colloid Interface Sci 244:342–346

Chai L, Wang Y, Zhao N, Yang W, You X (2013) Sulfate-doped Fe nanoparticles as a novel adsorbent for fluoride removal from drinking water. Water Res 47(12):4040–4049

Cheng J, Meng X, Jing C, Hao J (2014) La^{3+}-modified activated alumina for fluoride removal from water. J Hazard Mater 278:343–349

Chidambaram S, Ramanathan AL, Vasudevan S (2003) Fluoride removal studies in water using natural materials. Water SA 29:339–344

Coruh S, Ergun ON (2009) Ni^{2+} removal from aqueous solutions using conditioned clinoptilolites: kinetic and isotherm studies. Environ Prog Sustain Energy 28:162–172

Daifullah AAM, Yakout SM, Elreefy SA (2007) Adsorption of fluoride in aqueous solutions using $KMnO_4$-modified activated carbon derived from steam pyrolysis of rice straw. J Hazard Mater 147(1–2):633–643

Dong S, Wang Y (2016) Characterization and adsorption properties of a lanthanum-loaded magnetic cationic hydrogel composite for fluoride removal. Water Res 88(852):860

Fan X, Parker DJ, Smith MD (2003) Adsorption kinetics of fluoride on low cost materials. Water Res 37(20):4929–4937

Figueiredo SA, Loureiro JM, Boaventura RA (2005) Natural waste materials containing chitin as adsorbents for textile dyestuffs: batch and continuous studies. Water Res 39:4142–4152

Gao S, Sun R, Wei Z, Zhao H, Li H, Hu F (2009) Size-dependent defluoridation properties of synthetic hydroxyapatite. J Fluor Chem 130(6):550–556

Ghasemi Z, Younesi H (2011) Preparation and characterization of nanozeolite NaA from rice husk at room temperature without organic addictives. J Nanomater 2011:858961. https://doi.org/10.1155/2011/858961

Ghorai S, Pant KK (2005) Equilibrium, kinetics and breakthrough studies for adsorption of fluoride on activated alumina. Sep Purif Technol 42:265–271

Hammouda SB, Adhoum N, Monser L (2015) Synthesis of magnetic alginate beads based on Fe_3O_4 nanoparticles for the removal of 3-methylindole from aqueous solution using Fenton process. J Hazard Mater 294:128–136

Iyenger L (2005) Defluoridation of water using activated alumina technology. Indian Institute of Technology, Kanpur for UNICEF, New Delhi

Jagtap S, Yenkie MK, Das S, Rayalu S (2011) Synthesis and characterization of lanthanum impregnated chitosan flakes for fluoride removal in water. Desalination 273:267–275

Karthikeyan M, Kumar KKS, Elango KP (2011) Batch sorption studies on the removal of fluoride ions from water using eco-friendly conducting polymer/bio-polymer composites. Desalination 267:49–56

Kirk O (1980) Encyclopaedia of chemical technology, vol 10, 3rd edn. Wiley, New York

Lahnid S, Tahaikt M, Elaroui K, Elmidaoui A (2008) Economic evaluation of fluoride removal by electrodialysis. Desalination 230(1–3):213–219

Langmuir I (1915) The constitution and fundamental properties of solids and liquids. Part II. Liquids. J Am Chem Soc 38(5):102–105

Liu J, Xu Z, Li X, Zhang Y, Zhou Y, Wang Z, Wang X (2007) An improved process to prepare high separation performance PA/PVDF hollow fiber composite nanofiltration membranes. Sep Purif Technol 58(1):53–60

Liu B, Wang D, Yu G, Meng X (2013) Removal of F^- from aqueous solution using Zr (IV) impregnated dithiocarbamate modified chitosan beads. Chem Eng J 228:224–231

Maity JP, Hsu C, Lin T, Lee W, Bhattacharya P, Bundschuh J, Chen C (2018) Removal of fluoride from water through bacterial-surfactin mediated novel hydroxyapatite nanoparticle and its efficiency assessment: adsorption isotherm, adsorption kinetic and adsorption thermodynamics. Environ Nanotechnol Monit Manag 9:18–28

Meenakshi S, Viswanathan N (2007) Identification of selective ion-exchange resin for fluoride sorption. J Colloid Interface Sci 308(2):438–450

Mohapatra D, Mishra D, Mishra SP, Roy Chaudhury G, Das RP (2004) Use of oxide minerals to abate fluoride from water. J Colloid Interface Sci 275:355–359

Mukherjee S, Halder G (2016) Assessment of fluoride uptake performance of raw biomass and activated biochar of *Colocasia esculenta* stem: optimization through response surface methodology. Environ Prog Sustain Energy 35(5):1305–1316

Mukherjee S, Halder G (2018) A review on the sorptive elimination of fluoride from contaminated wastewater. J Environ Chem Eng 6(1):1257–1270

Mukherjee S, Mondal M, Banerjee S, Halder G (2017) Elucidation of the sorptive uptake of fluoride by Ca^{2+}- treated and untreated algal biomass of *Nostoc* sp. (BTA394): isotherm, kinetics, thermodynamics and safe disposal. Process Saf Environ Protect 107:334–345

Mukherjee S, Dutta S, Ray S, Halder G (2018a) A comparative study on defluoridation capabilities of biosorbents: isotherm, kinetics, thermodynamics, cost estimation and eco-toxicological study. Environ Sci Pollut Res 25(18):473–489

Mukherjee S, Barman S, Halder G (2018b) Fluoride uptake by zeolite NaA synthesized from rice husk: isotherm, kinetics, thermodynamics and cost estimation. Groundw Sustain Dev 7:39–47

Onyango MS, Kojima Y, Aoyi O, Bernardo EC, Matsuda H (2004) Adsorption equilibrium modeling and solution chemistry dependence of fluoride removal from water by trivalent-cation-exchanged zeolite F-9. J Colloid Interface Sci 279:341–350

Paudyal H, Pangeni B, Ghimire KN, Inoue K, Ohto K, Kawakita H, Alam S (2012) Adsorption behavior of orange waste gel for some rare earth ions and its application to the removal of fluoride from water. Chem Eng J 195:289–296

Pradhan J, Das SN, Thakur RS (1999) Adsorption of hexavalent chromium from aqueous solution by using activated red mud. J Colloid Interface Sci 217(1999):137–141

Qiusheng Z, Xiaoyan L, Jin Q, Jing W, Xuegang L (2015) Porous zirconium alginate beads adsorbent for fluoride adsorption from aqueous solutions. RSC Adv 5:2100–2112

Ramos RL, Ovalle-Turrubiartes J, Sanchez-Castillo MA (1999) Adsorption of fluoride on aluminium impregnated carbon. Carbon 37:609–617

Rocher V, Beea A, Siaugue J, Cabuil V (2010) Dye removal from aqueous solution by magnetic alginate beads crosslinked with epichlorohydrin. J Hazard Mater 178:434–439

Santra D, Joarder R, Sarkar M (2014) Taguchi design and equilibrium modeling for fluoride adsorption on cerium loaded cellulose nanocomposite bead. Carbohydr Polym 111:813–821

Sehn P (2008) Fluoride removal with extra low energy reverse osmosis membranes: three years of large scale field experience in Finland. Desalination 223(1–3):73–84

Srimurali M, Pragathi A, Karthikeyan J (1998) A study on removal of fluorides from drinking water by adsorption onto low-cost materials. Environ Pollut 99:285–289

Tomar V, Prasad S, Kumar D (2013) Adsorptive removal of fluoride from water samples using Zr–Mn composite material. Microchem J 111:116–124

Tor A (2006) Removal of fluoride from an aqueous solution by using montmorillonite. Desalination 201:267–276

Tor A (2007) Removal of fluoride from water using anion-exchange membrane under Donnan dialysis condition. J Hazard Mater 141(3):814–818

Travlou NA, Kyzas GZ, Lazaridis NK, Deliyanni EA (2013) Graphite oxide/chitosan composite for reactive dye removal. Chem Eng J 217:256–265

Vázquez G, Mosquera O, Freire MS, Antorrena G, González-Álvarez J (2012) Alkaline pre-treatment of waste chestnut shell from a food industry to enhance cadmium, copper, lead and zinc ions removal. Chem Eng J 184:147–155

Wang WD, Feng YL, Tang XH, Li HR, Du ZW, Yi AF, Zhang X (2015) Enhanced U(VI) bioreduction by alginate immobilized uranium-reducing bacteria in the presence carbon nanotubes and anthraquinone-2,6-disulfonate. J Environ Sci 69:68–73

Wu FC, Tseng RL, Juang RS (2001) Enhanced abilities of highly swollen chitosan beads for color removal and tyrosinase immobilization. J Hazard Mater 81(1):167–177

Yakun H, Wenming D, Menghua Z, Xia H, Jingnian X (2011) Fluoride removal by lanthanum alginate bead: adsorbent characterization and adsorption mechanism. Chin J Chem Eng 19(3):365–370

Yu X, Tong S, Ge M, Zuo J (2013) Removal of fluoride from drinking water by cellulose @ hydroxyapatite nanocomposites. Carbohydr Polym 92(1):269–275

Yu J, Wang J, Jiang Y (2017) Removal of uranium from aqueous solution by alginate beads. Nucl Eng Technol 49:534–540

Zhang S, Lu Y, Lin X, Su X, Zhang Y (2014) Removal of fluoride from groundwater by adsorption onto La (III)-Al (III) loaded scoria adsorbent. Appl Surf Sci 303:1–5